COMMUNICATION

Check for updates

Re-engineered theranostic gold nanoparticles for targeting tumor hypoxia†

Sweety Mittal, [ID] [a] Chandan Kumar,[a] Madhava B. Mallia [ID] *[ab] and Haladhar Dev Sarma[c]

Developing nanovehicles for selective delivery of a radiation dose/drug to hypoxic tumors is a present-day clinical requirement for effective treatment of cancer. Herein, we describe our attempt to re-engineer the earlier reported lipoic acid-capped ^{177}Lu-labeled nitroimidazole-decorated gold nanoparticles to favorably modulate their pharmacokinetics to reduce uptake in the reticuloendothelial system while retaining the uptake in tumors. Towards this, gold nanoparticles with PEG-chains terminated with 2-nitroimidazole and Bz-DOTA were synthesized [(DOTA)AuNP-PEG-2K-(2-NIM)]. Surface modification of the gold nanoparticles with PEG-2K and 2-nitroimidazole was confirmed through infrared spectroscopy. The conjugation of Bz-DOTA on the nanoparticle surface was confirmed by UV-Vis spectroscopy, which showed a peak at 260−280 nm corresponding to Bz-DOTA. The DLS analysis of gold nanoparticles showed an effective hydrodynamic diameter of 28.9 ± 1.50 nm with a zeta potential value of -20.62 ± 0.05 mV at pH 7.4. The nanoparticles were radiolabeled with lutetium-177 with >98% radiochemical purity. *In vitro* studies using radiolabeled nanoparticles ([^{177}Lu]Lu-(DOTA)AuNP-PEG-2K-(2-NIM)) in CHO cells showed their 2-fold uptake under hypoxic conditions (at 4 h post incubation) compared to the radiolabeled nanoparticles without nitroimidazole units. The hypoxia selective uptake of the nanoparticles was further confirmed by flow cytometry using a fluorescent analogue (DOTA)AuNP-PEG-2K-(2-NIM)(FITC). It was, however, observed that hypoxic cell uptake of the PEG-2K capped nanoparticles was lower than that of their lipoic acid capped counterpart. *In vivo* biodistribution studies in tumor bearing Swiss

[a] *Radiopharmaceuticals Division, Bhabha Atomic Research Centre, Trombay, Mumbai-400085, India. E-mail: sweetys@barc.gov.in, ckumar@barc.gov.in, hdsarma@barc.gov.in*

[b] *Homi Bhabha National Institute, Anushaktinagar, Mumbai-400094, India. E-mail: mallia@barc.gov.in; Fax: +91 22 2550 5151; Tel: +91 22 25590746*

[c] *Radiation Biology and Health Sciences Division, Bhabha Atomic Research Centre, Mumbai-400085, India*

† Electronic supplementary information (ESI) available: Materials and methods used for the synthesis of ligands, characterization data of the ligands such as IR, ^{1}H NMR, ^{13}C NMR and ESI-MS, radiolabeling procedure, quality control of the radiotracer, *etc.* See DOI: https://doi.org/10.1039/d3ma00679d

mice demonstrated that PEGylation of nanoparticles could significantly reduce the uptake in the RES while retaining uptake in tumors albeit to a lesser extent.

Hypoxia is a hallmark of locally advanced solid tumors wherein the localized region with low oxygen concentration develops within the tumor mass due to poor vasculature. To adapt to this hostile microenvironment, cellular response to hypoxia gets activated through the transcriptional activity of hypoxia-inducible factors (HIFs), which leads to expression of multiple genes involved in glucose metabolism, angiogenesis, cell invasion and metastasis.[1] Hypoxia in tumors is associated with failure of therapy (both chemotherapy and radiotherapy), recurrence of the disease, and therefore, has been identified as a negative prognostic factor in clinical management of cancer.[2,3] Development of clinical strategies for efficient mapping of hypoxia in tumors along with hypoxia targeted therapies to improve overall therapeutic outcome is an active area of research.[4−8]

Various approaches, invasive as well as non-invasive, are available for mapping hypoxia in tumors.[9−11] Non-invasive methods of mapping hypoxia mainly involve the use of gamma or positron emitting radiopharmaceuticals. Mapping of hypoxic regions in tumors is followed by hypoxia directed therapy for clinical management of the disease.[12,13] Various hypoxia-directed therapeutic modalities, including hypoxia directed external beam radiation therapy, are reviewed elsewhere.[14,15] However, studies involving the use of therapeutic radiopharmaceuticals for hypoxia directed radiotherapy are limited.[16,17] Development of non-invasive methods, such as the use of targeted therapeutic radiopharmaceuticals, may have advantages over hypoxia directed external beam radiation therapy. While targeted therapeutic radiopharmaceuticals can accumulate in all hypoxic tumor tissues upon intravenous administration, external beam radiation therapy may require focusing a beam on hypoxic sites in individual tumor lesions, if multiple tumors are present. The primary requirement for developing such targeted therapeutic radiopharmaceuticals is the availability of a molecular vehicle that could selectively target hypoxic tumor cells.

Nanomaterials, given their high surface to volume ratio, are ideal platforms to achieve multiple objectives such as targeting hypoxic cells, carrying suitable radioisotopes for diagnosis or therapy or carrying chemotherapeutic drugs. Furthermore, nanoparticles have an inherent tendency to accumulate in solid tumors *via* the enhanced permeability and retention effect (EPR), which originates from a leaky vasculature and poor lymphatic drainage in tumor tissues.[18] Among various metallic nanoparticles, gold nanoparticles, considering their biocompatibility, easy synthesis and facile surface functionalization, are a preferred candidate for targeted applications and have been extensively investigated in the recent past.[19–23]

Nitroimidazole derivatives with their unique response to a hypoxic environment have been extensively exploited as non-invasive probes to target hypoxic tumor cells. They undergo irreversible, oxygen dependent, enzymatic reduction and accumulation in hypoxic cells. With the first step being reversible under normoxic conditions, accumulation in normal cells is insignificant. A nitroimidazole derivative tagged with a gamma/positron emitting radioisotope can thus be used as a sensitive marker for detecting hypoxic cells *in vivo*. We had evaluated lutetium-177-labeled, 2-nitroimidazole-decorated gold nanoparticles for targeting hypoxia in tumors.[23] The *in vitro* studies in CHO cells showed more than 9-fold accumulation of the radiotracer under hypoxic conditions compared to normoxic conditions. *In vivo* studies in solid tumor bearing mice also showed uptake and retention of the radiotracer in tumors. However, significant uptake in the reticuloendothelial system (RES) presented a drawback. Concluding that study, we had opined that PEGylation (PEG – polyethylene glycol) of the nanoparticles could be a way forward to minimize the uptake of the radiotracer in the RES.[23] Surface modification with PEG has been a widely used strategy to inhibit aggregation, increase *in vivo* stability of nanoparticles, prevent non-specific protein adsorption on nanoparticle surfaces and to reduce uptake by the RES. Utilizing this prior knowledge, in the present work, we re-engineered the nanoparticle surface with PEG units instead of lipoic acid units, in an attempt to reduce uptake by the RES while retaining the favorable hypoxia targeting properties of the earlier reported nitroimidazole decorated nanoplatform. The free-end of the PEG-chains was used to tether nitroimidazole units to impart hypoxia selectivity and DOTA units are conjugated to enable radiolabeling with a suitable radioisotope. As reported in a previous study, $[^{177}Lu]Lu$ ($t_{1/2}$ = 6.7 days) was chosen, which is an ideal radioisotope for theranostic applications.[24] It has simultaneous emission of gamma photons [208 keV (11%) and 112 keV (6.4%)] for imaging and beta emissions $[E_{\beta_{max}} = 0.49$ MeV] to impart therapy. Optically traceable nanoparticles were synthesized by conjugating fluorescein isothiocyanate (FITC) to the 2-NIM decorated nanoparticles to study their cellular localization by flow cytometry and fluorescence cell imaging under both hypoxic and normoxic conditions.

While PEGylation of nanoparticles is an established strategy to develop drug delivery systems,[25–27] the impact of PEGylation on cellular uptake of the nanoparticles is less known. Bo He *et al.* observed insignificant uptake of gold nanoparticles

modified with PEG2000 in A549 cells.[28] However, upon modification with certain peptides at the free end of PEG2000, cellular uptake increased significantly. Lok Wai Cola Ho *et al.* studied the effect of alkylation at the distal end of the PEG5000 modified gold nanoparticles and found that alkylation helps internalization of the gold nanoparticles in Kera-308 keratinocytes.[29] The authors observed that the degree of internalization was dependent on the length of the alkyl chain as well as the number of alkyl chains per PEGylated gold nanoparticle. This possibly indicates that leaving the distal end of the PEG-chain free is not favorable as far as cellular uptake is concerned. The gold nanoparticles reported herein had the distal end of the PEG2000 modified either with 2-nitroimidazole or DOTA, and therefore, we expect no hindrance to the cellular uptake. The present study reports the preparation, evaluation and the results obtained with ^{177}Lu-labeled nitroimidazole decorated PEGylated nanoparticles designed for targeting hypoxic tumor cells.

Earlier reported $[^{177}Lu]$-labeled gold nanoparticles surface modified with lipoic acid showed excellent hypoxia selectivity (more than 9-fold) in CHO cells *in vitro*.[23] However, significant uptake in the RES prompted us to look for modifications to reduce or eliminate this unfavorable *in vivo* behavior of the radiotracer. In the literature, PEGylation of nanoparticles was found to be helpful in minimizing the uptake by the RES.[30,31] Therefore, a PEGylated, nitroimidazole-decorated, lutetium-177-labeled gold nanoplatform was envisaged.

The scheme followed for the synthesis of $[^{177}Lu]Lu$-DOTA-AuNP-PEG-2K-(2-NIM) is shown in Fig. 1(a). The 2-(2-nitro-1*H*-imidazol-1-yl)acetic acid (**2**) was synthesized by a two-step reaction sequence. Deprotection of the *tert*-butyl ester derivative of 2-nitroimidazole prepared in step 1 (**1**) was carried out using TFA to obtain the corresponding carboxylic acid derivative (**2**) in quantitative yield. Both compounds (**1**) and (**2**) were characterized by appropriate spectroscopic techniques [Fig. S1–S4 in the ESI†]. The change in the carbonyl peak position from 1741 cm^{-1} (s) in 2-nitroimidazole *tert*-butyl ester to 1729 cm^{-1} along with the appearance of a broad weak peak at 3500 cm^{-1} indicate the formation of compound **2** [Fig. S5 in the ESI†]. The disappearance of a singlet at 1.47 δ ppm, corresponding to the nine methyl protons of the *tert*-butyl acetate group, in the ^{1}H-NMR/^{13}C-NMR spectrum of the compound **2** and a molecular ion peak at *m/z* 172.03 (M + H)$^+$ in the mass spectrum of 2-(2-nitro-1*H*-imidazol-1-yl)acetic acid (**2**) provides additional evidence for its formation [Fig. S6–S8 in the ESI†]. PEG-2K tagged gold nanoparticles (AuNP-PEG-2K-NH$_2$) were synthesized by the reduction of gold salt (HAuCl$_4$·3H$_2$O) with sodium borohydride (NaBH$_4$) [Fig. 1(b)] in the presence of three times excess of SH-PEG-2K-NH$_2$ with respect to gold salt. The gold nanoparticles were purified by centrifugal filtration using an Amicon Ultra centrifugal filter (MWCO 3 KDa) followed by characterization using DLS, UV-Vis, FT-IR and TEM. The presence of a typical SPR band at ~520 nm in the UV-Vis spectrum indicates the formation of gold nanoparticles [Fig. 2(a)]. The presence of a strong C–O stretching peak at 1090 cm^{-1} in the IR spectrum of AuNP-PEG-2K-NH$_2$ along with the aliphatic C–H stretching frequency peak at 2870 cm^{-1} confirm the immobilization of PEG units on the gold
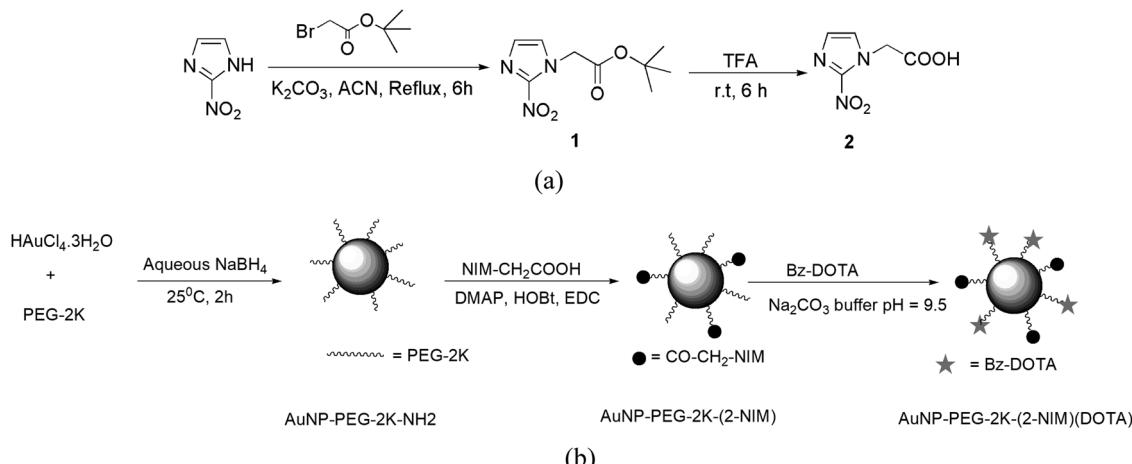
Fig. 1 (a) Synthesis of 2-(2-nitro-1H-imidazol-1-yl)acetic acid (**2**). (b) Synthesis of (DOTA)AuNP-PEG-2K-(2-NIM).

nanoparticle surface [Fig. S9 in the ESI†]. The conjugation of 2-(2-nitro-1H-imidazol-1-yl)acetic acid (**2**) with the amine group of PEG tagged gold nanoparticles was carried out using HOBt, EDC and DMAP. After purification by centrifugal filtration, the IR spectrum of the nanoparticles showed emergence of a carbonyl stretching frequency peak at 1640 cm^{-1} confirming the attachment of the 2-nitroimidazole moiety to the nanoparticles [Fig. S9 in the ESI†]. The conjugation of Bz-DOTA on the nanoparticle [AuNP-PEG-2K-(2-NIM)] surface was accomplished through thiourea bond formation under basic conditions (0.01 M carbonate buffer, pH 9.5). The overlaid UV-Vis spectrum of gold nanoparticles after conjugation with 2-nitroimidazole and DOTA is shown in [Fig. 2(b)].

The signature peaks of 2-NIM and Bz-DOTA in the UV-Vis spectrum of (DOTA)AuNP-PEG-2K-(2-NIM) confirm their presence in the nanoparticle surface.

The TEM images showed nanoparticles were nearly of uniform size with average particle sizes of 5 ± 1.2 nm (**3**), 10 ± 1.8 nm (**4**) and 20 ± 1.5 nm (**5**) [Fig. 3(a)] for AuNP-PEG-2K-NH$_2$, AuNP-PEG-2K-(2-NIM) and (DOTA)AuNP-PEG-2K-(2-NIM), respectively.

Similarly, the DLS analysis of particles showed an effective hydrodynamic diameter of nm, 8.5 ± 1.14 nm, 14.9 ± 1.23 and 28.9 ± 1.50 nm for AuNP-PEG-2K-NH$_2$, AuNP-PEG-2K-(2-NIM) and (DOTA)AuNP-PEG-2K-(2-NIM), respectively, with a low polydispersity index [Fig. 3(b)]. The zeta potential value of the nanoparticles was found to be 28.5 ± 0.99 mV, 22.92 ± 0.45 mV and -20.62 ± 0.05 mV for the preparations **3**, **4** and **5**, respectively, at pH 7.4. The gradual increase in the size of gold nanoparticles could be attributed to the increase in the shell-volume resulting from the sequential modification of the nanoparticle surface with PEG units with 2-nitroimidazole and DOTA. Similar observations were reported by Gu *et al.* when citrate stabilized gold nanoparticles (AuNPs; 8.2 ± 0.6 nm) were sequentially modified to PEGylated gold nanoparticles (Au-PEG; 16.2 ± 0.4 nm) and further to Doxorubicin-loaded PEGylated gold nanoparticles (Au-PEG-SS-DOX; 28.2 ± 0.2 nm).[32] Similarly, Mahalunkar *et al.* reported a significant increase in the size of curcumin loaded gold nanoparticles (CurAu-PVP NP; ~15 nm) upon conjugation of folic acid to PVP (FA-CurAu-PVP NPs; ~250 nm).[33]

In-house produced [^{177}Lu]LuCl$_3$ was used for radiolabeling the DOTA conjugated nanoparticles. The radiochemical purity
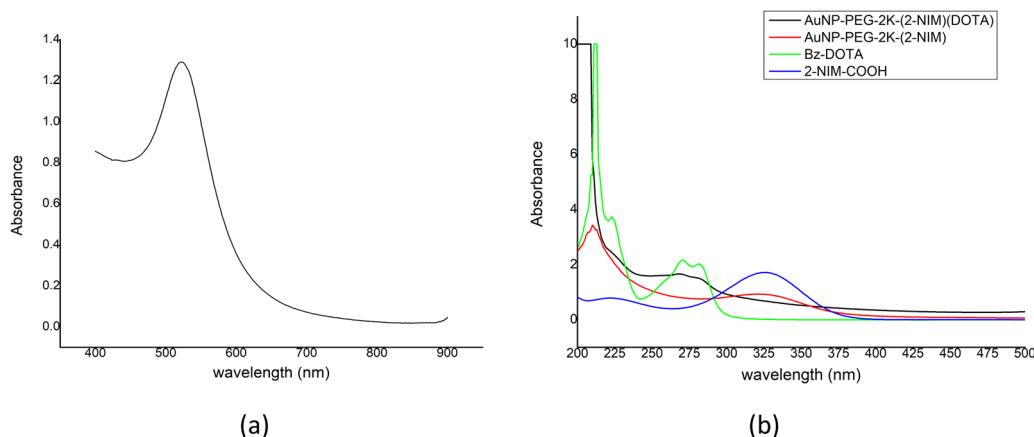
Fig. 2 (a) UV-Vis spectrum of AuNP-PEG-2K-NH$_2$. (b) Overlayed UV-Vis spectrum of AuNP-PEG-2K-NH$_2$(2-NIM)(DOTA), AuNP-PEG-2K-(2-NIM), Bz-DOTA and 2-NIM-COOH.
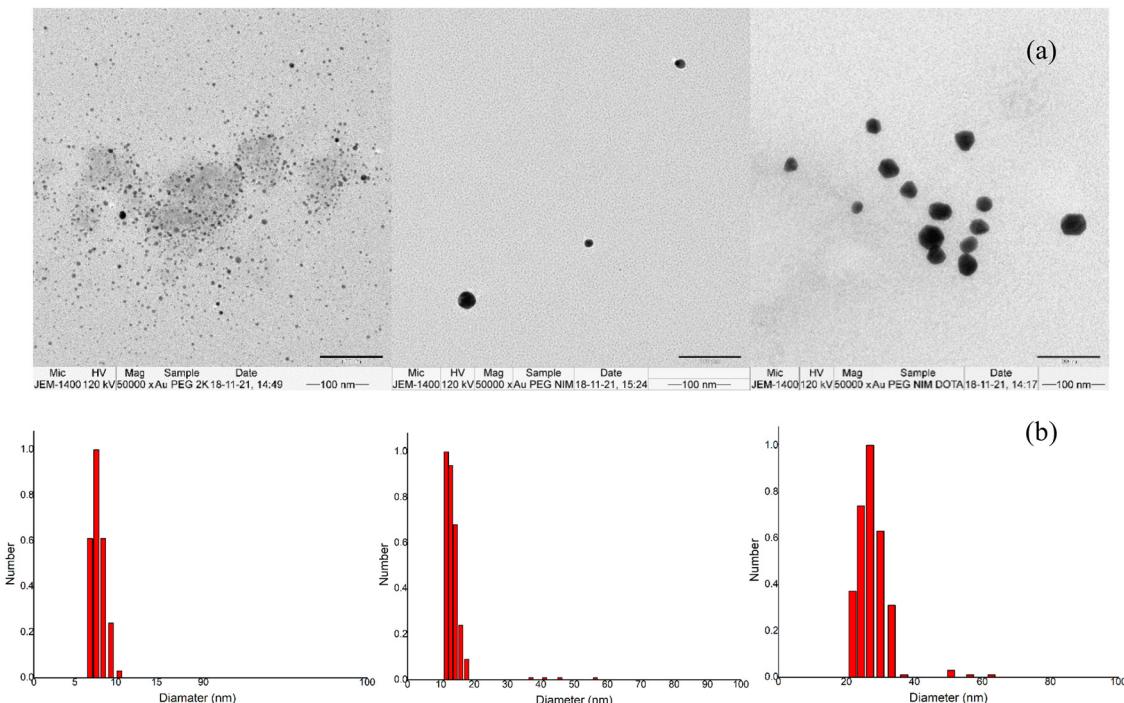
Fig. 3 (a) TEM images of AuNP-PEG-2K-NH$_2$, AuNP-PEG-2K-(2-NIM) and AuNP-PEG-2K-(2-NIM)(DOTA) [left to right]. (b) Size distribution data of AuNP-PEG-2K-NH$_2$, AuNP-PEG-2K-(2-NIM) and AuNP-PEG-2K-(2-NIM)(DOTA) [left to right].

(RCP) of the radiolabeled nanoparticles was determined by radio-TLC [Fig. S10 in the ESI†] in which the radiolabeled nanoparticles remained at the point of application (R_f = 0.0–0.1), while free [^{177}Lu]LuCl$_3$ migrated to the solvent front (0.7–1.0). The peak area measurements showed RCP of [^{177}Lu]Lu-(DOTA)AuNP-PEG-2K-(2-NIM) to be ∼92% before purification and >98% after purification using a PD-10 column. The RCP of the radiolabeled nanoparticles was further confirmed by size-exclusion chromatography using the PD-10 column. The radiolabeled nanoparticles were eluted in the 3rd and 4th fraction. The RCP determined by this method was in excellent agreement with that determined by the radio-TLC method. The specific activity of the radiolabeled preparation was ∼18.0 ± 1.85 μCi per μg.

In vitro stability of the radiolabeled nanoparticles was investigated both in human serum as well as in PBS over a period of one week by radio-TLC [Fig. S11 in the ESI†]. Over this period, the RCP of [^{177}Lu]Lu-(DOTA)AuNP-PEG-2K-(2-NIM) nanoparticles in PBS decreased marginally from 98 ± 2.5 to 96.41 ± 1.89%, while in human serum it decreased from 98.01 ± 2.68 to 94.12 ± 1.95%. These results indicate the high stability of radiolabeled nanoparticles in human serum as well as PBS.

Hypoxia selectivity of radiolabeled nanoparticles, [^{177}Lu]Lu-(DOTA)AuNP-PEG-2K-(2-NIM), was evaluated *in vitro* in CHO cells. The radiolabeled nanoparticles were incubated with CHO cells both under hypoxic conditions as well as normoxic conditions.[23,34] The results are presented in Fig. 4. It could be
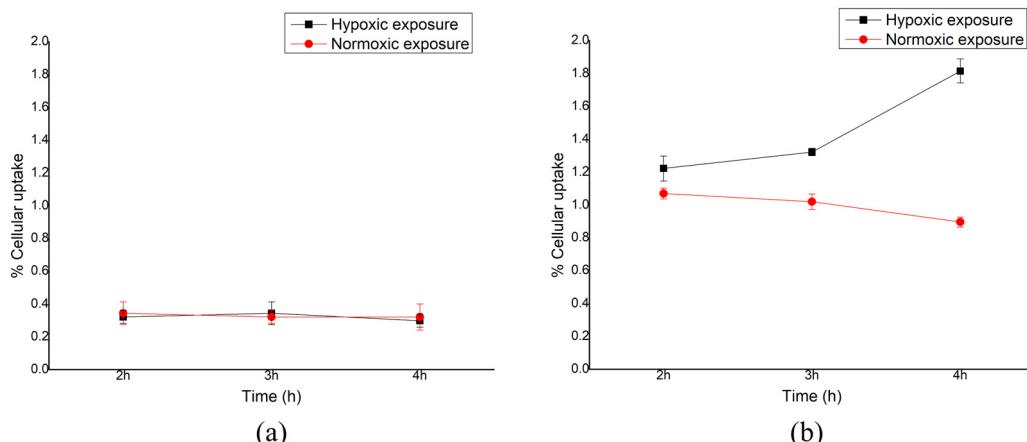
Fig. 4 *In vitro* cellular uptake of (a) control nanoparticles and (b) preparation under hypoxic and normoxic conditions.

observed that there is significant uptake of the radiotracer in CHO cells upon hypoxic exposure compared to normoxic exposure ($P < 0.02$, t-test) [Fig. 4(b)]. The hypoxic/normoxic ratio was 1.15 ± 0.10 at 2 h post-incubation with CHO cells, which increased to 2.02 ± 0.6 at 4 h post-incubation. For comparison, a similar experiment was performed with ^{177}Lu-labeled nanoparticle control, [^{177}Lu]Lu-(DOTA)-AuNP-PEG-2K, without the 2-nitroimidazole moiety [Fig. 4(a)]. The results clearly showed insignificant uptake of control nanoparticles either under hypoxic or normoxic conditions confirming the role of 2-nitroimidazole in hypoxia specific uptake. The hypoxic/normoxic ratio remained close to 1 over the period of study (0.94 ± 0.07, 1.06 ± 0.05 and 0.90 ± 0.12 at 2 h, 3 h and 4 h post incubation, respectively). The careful examination of the results indicated significant accumulation ($P < 0.01$, t-test) of nitroimidazole decorated gold nanoparticles under hypoxic conditions compared to control nanoparticles ([^{177}Lu]Lu-(DOTA)-AuNP-PEG-2K) where nitroimidazole units are absent. The studies, however, revealed that PEGylation of gold nanoparticles resulted in a hypoxic/normoxic ratio (two-fold) not as high as that of radiolabeled lipoic acid coated gold nanoparticles (9 fold) reported by us earlier[23] under similar experimental conditions. Torrissi

et al. had reported a similar observation with PEGylated iron oxide nanoparticles.[35] However, they observed this behavior with an iron oxide nanoparticle surface modified with polyphosphonic acid-PEG copolymers where the distal end of the PEG chains are free. As mentioned earlier, this is similar to the insignificant uptake of gold nanoparticles modified with PEG2000 observed by Bo He et al.[28] Christina Brandenberger et al. reported a similar observation wherein lower intracellular uptake of citrate capped and PEG capped gold nanoparticles was observed in A549 cells. Interestingly, the presence of the latter was found to be more than the former in the cytosol of the cell.[36] It is pertinent to note that PEGylated gold nanoparticles with the distal end of PEG-units tagged with 2-nitroimidazole or DOTA showed significant uptake in cells under hypoxic conditions albeit lower than lipoic acid coated gold nanoparticles.

To further establish the hypoxia selectivity of (DOTA)AuNP-PEG-2K-(2-NIM) nanoparticles, fluorescent gold nanoparticles (DOTA)AuNP-PEG-2K-(2-NIM)(FITC) were synthesized. The FITC tagged nanoparticles were incubated with CHO cells under both hypoxic and normoxic conditions. Flow cytometry analysis of the cells incubated for 4 h under hypoxic conditions showed
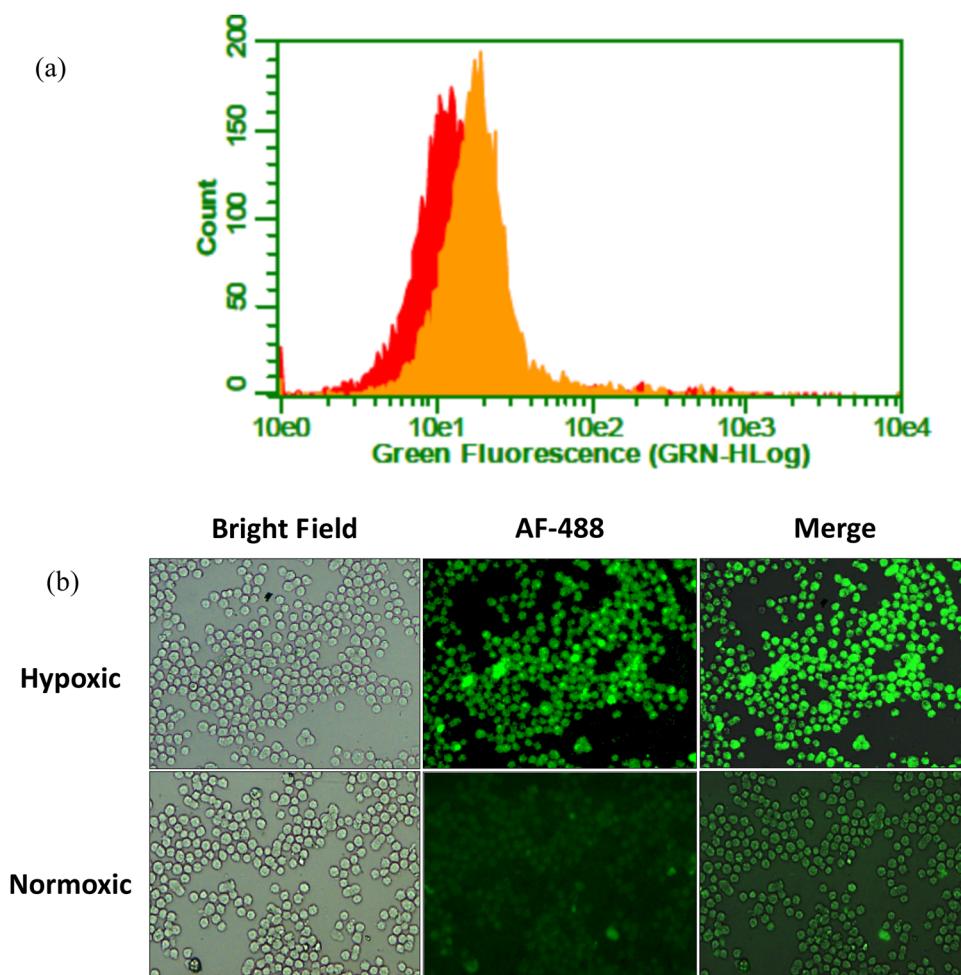
Fig. 5 (a) Flow cytometry histogram profile of CHO cells treated with FITC tagged gold nanoparticles (DOTA)AuNP-PEG-2K-(2-NIM) (FITC) under hypoxic (orange) and normoxic (red) conditions. (b) Bright field and fluorescence images of CHO cells incubated with (DOTA)AuNP-PEG-2K-(2-NIM) (FITC) under hypoxic and normoxic conditions.

Table 1 Distribution of [^{177}Lu]Lu-DOTAGA-AuNP-2-NIM in different organs/tissues

Organs	% Injected dose per gram Avg. (s.d.)[b]		
	2 h	4 h	24 h
Liver	0.24 (0.04)	0.05 (0.15)	0.04 (0.02)
Intestine	0.06 (0.01)	0.06 (0.03)	0.00 (0.00)
Stomach	0.15 (0.08)	0.02 (0.01)	0.00 (0.01)
Kidney	0.81 (0.15)	0.35 (0.25)	0.10 (0.01)
Heart	0.29 (0.08)	0.02 (0.05)	0.00
Lungs	0.39 (0.09)	0.04 (0.01)	0.01 (0.02)
Spleen	0.05 (0.08)	0.00 (0.03)	0.00 (0.02)
Blood	0.41 (0.04)	0.09 (0.00)	0.00
Muscle	0.11 (0.02)	0.00 (0)	0.00
Tumor	**0.13 (0.01)**	**0.04 (0.01)**	**0.02 (0.00)**
Excretion[a]	75.91 (3.46)	87.10 (1.27)	90.31 (8.09)
Tumor/blood ratio	0.31 (0.02)	0.44 (0.08)	Very high
Tumor/muscle ratio	1.18 (0.51)	Very high	Very high

[a] Excretion is calculated by adding percentage of the injected dose in all organs and then subtracting from 100. [b] s.d. – standard deviation.

[Fig. 5(a)] a fluorescence signal shift with a MFI of 21.7 ± 0.97 (a peak marked in orange) indicating enhanced retention of (DOTA)AuNP-PEG-2K-(2-NIM)(FITC) compared to the cells incubated under normoxic conditions [MFI 17.8 ± 1.18 (a peak marked in red)]. The flow histogram [Fig. S12 in the ESI†] shows a significant increase in the population of CHO cells with green fluorescence under hypoxic conditions compared to normoxic conditions at 4 h post incubation. These observations are in concordance with the results obtained with ^{177}Lu-labeled nanoparticles. The fluorescence images of the CHO cells treated with (DOTA)AuNP-PEG-2K-(2-NIM)(FITC) under hypoxic and normoxic conditions for 4 h convincingly revealed the preferential uptake of nanoparticles under hypoxic conditions compared to normoxic conditions, corroborating the results obtained with ^{177}Lu-labeled nanoparticles and flow cytometry [Fig. 5(b)].

Biodistribution studies were carried out in Swiss mice bearing fibrosarcoma tumors. Distribution of the radiotracer in different organs/tissues is shown in Table 1. The radiotracer cleared quickly from the body, which had a significant impact on the uptake of the radiotracer in tumors. Approximately 75% of the activity initially administered in the animal was excreted within 2 h after injection. We had a similar observation with other radiotracers evaluated for targeting tumor hypoxia.[34,37,38] Fast clearance of activity from blood (0.41% ID per g at 2 h p.i. and 0.09% ID per g at 4 h p.i.) resulted in limited uptake and retention in tumors (0.13% ID per g at 2 h p.i. and 0.04% ID per g at 4 h p.i.). Consequently there was a significant decrease in activity in tumors between 2 h and 4 h p.i. ($P < 0.01$, t-test) and between 4 h and 24 h ($P < 0.05$, t-test). The radiotracer requires some time to distribute across tumor mass and undergo hypoxia selective reduction, which is denied due to fast clearance of the radiotracer from blood.[39] Though quick clearance of the radiotracer from the body is considered to be a virtue for radiopharmaceuticals, in this case it has resulted in reduced uptake in tumors. Reduction in non-specific binding to serum proteins due to PEGylation must have assisted the faster clearance

of the radiotracer from blood. There was no significant uptake of the radiotracer in liver (0.24% ID per g at 2 h p.i.) and spleen (0.05% ID per g at 2 h p.i.) contrary to the lipoic acid coated gold nanoparticles reported earlier (13.57% ID per g in liver and 1.97% ID per g in spleen at 3 h p.i.) ($P < 0.02$, t-test).[23] The increase in the tumor/blood ratio between 2 h and 4 h is not significant ($P > 0.05$, t-test). However, very high tumor to blood and tumor to muscle ratios were observed at 24 h p.i. PEGylation of nanoparticles has been an extensively used strategy to increase the blood circulation time and to decrease the uptake in the RES by the stealth effect.[40,41] Similar to the previous reports a significant decrease in the uptake of radiolabeled nanoparticles in the RES was observed in the present study as well, however, an improvement in the blood circulation time was not observed.

Several factors like size, charge and surface chemistry of nanoparticles (such as the chain length and conformation of PEG molecules on the nanoparticle surface), intricately play an important role in determining the cellular uptake, immune system activation and overall pharmacokinetics.[42] It is generally accepted that nanoparticles with less than 5 nm diameter can only be cleared via kidneys (glomerular filtration cut off) while larger nanoparticles (size more than 100 nm) do not accumulate in kidneys.[43,44] However, there are some reports indicating larger nanoparticles with size 100–200 nm undergoing renal clearance through an alternative mechanism, although the mechanism is not clear yet.[45] The effective size of (DOTA)AuNP-PEG-2K-(2-NIM) reported herein was 28.9 ± 1.50 nm and major clearance was observed through kidneys. It seems the PEG capping on the nanoparticles further enhances the renal clearance compared to non-PEGylated nanoparticles which are mainly taken up by the RES.[46]

Conclusion

The present work describes the preparation and biological evaluation of hypoxic cell-targeting radiolabeled, 2-nitroimidazole-decorated gold nanoparticles capped with PEG-2k units. In vitro, the nanoparticles showed hypoxia selectivity in CHO cells albeit to a lesser extent than the lipoic acid modified analogue reported earlier. In vivo, our attempt to reduce the uptake in the RES was successful, but the modification was found to be not favorable for retaining the tumor uptake. Careful analysis of the results points to very fast clearance of the radiotracer as a possible reason for the low uptake and retention in tumors in vivo despite showing hypoxia selectivity in vitro. The nanoplatform reported requires further tuning to combine the favorable pharmacokinetics while retaining high hypoxia selectivity.

Conflicts of interest

The authors declare no competing interest.

Acknowledgements

References

1 M. Filippi, D.-V. Nguyen, F. Garello, F. Perton, S. Bégin-Colin, D. Felder-Flesch, L. Power and A. Scherberich, Metronidazole-Functionalized Iron Oxide Nanoparticles for Molecular Detection of Hypoxic Tissues, *Nanoscale*, 2019, **11**(46), 22559–22574, DOI: **10.1039/C9NR08436C**.

2 W. Zeng, P. Liu, W. Pan, S. R. Singh and Y. Wei, Hypoxia and Hypoxia Inducible Factors in Tumor Metabolism, *Cancer Lett.*, 2015, **356**(2), 263–267, DOI: **10.1016/j.canlet.2014.01.032**.

3 L. Liu, X. Ning, L. Sun, H. Zhang, Y. Shi, C. Guo, S. Han, J. Liu, S. Sun, Z. Han, K. Wu and D. Fan, Hypoxia-Inducible Factor-1 Alpha Contributes to Hypoxia-Induced Chemoresistance in Gastric Cancer, *Cancer Sci.*, 2008, **99**(1), 121–128, DOI: **10.1111/j.1349-7006.2007.00643.x**.

4 M. I. Confeld, B. Mamnoon, L. Feng, H. Jensen-Smith, P. Ray, J. Froberg, J. Kim, M. A. Hollingsworth, M. Quadir, Y. Choi and S. Mallik, Targeting the Tumor Core: Hypoxia-Responsive Nanoparticles for the Delivery of Chemotherapy to Pancreatic Tumors, *Mol. Pharm.*, 2020, **17**(8), 2849–2863, DOI: **10.1021/acs.molpharmaceut.0c00247**.

5 H. Xu, Y. Han, G. Zhao, L. Zhang, Z. Zhao, Z. Wang, L. Zhao, L. Hua, K. Naveena, J. Lu, R. Yu and H. Liu, Hypoxia-Responsive Lipid–Polymer Nanoparticle-Combined Imaging-Guided Surgery and Multitherapy Strategies for Glioma, *ACS Appl. Mater. Interfaces*, 2020, **12**(47), 52319–52328, DOI: **10.1021/acsami.0c12971**.

6 D. Sarkar, M. Chowdhury and P. K. Das, Naphthalimide-Based Azo-Functionalized Supramolecular Vesicle in Hypoxia-Responsive Drug Delivery, *Langmuir*, 2022, **38**(11), 3480–3492, DOI: **10.1021/acs.langmuir.1c03334**.

7 B. Mamnoon, J. Loganathan, M. I. Confeld, N. De Fonseka, L. Feng, J. Froberg, Y. Choi, D. M. Tuvin, V. Sathish and S. Mallik, Targeted Polymeric Nanoparticles for Drug Delivery to Hypoxic, Triple-Negative Breast Tumors, *ACS Appl. Bio Mater.*, 2021, **4**(2), 1450–1460, DOI: **10.1021/acsabm.0c01336**.

8 M. R. Horsman, B. S. Sørensen, M. Busk and D. W. Siemann, Therapeutic Modification of Hypoxia, *Clin. Oncol.*, 2021, **33**(11), e492–e509, DOI: **10.1016/j.clon.2021.08.014**.

9 P. Vaupel and A. Mayer, Hypoxia in Cancer: Significance and Impact on Clinical Outcome, *Cancer Metastasis Rev.*, 2007, **26**(2), 225–239, DOI: **10.1007/s10555-007-9055-1**.

10 M. Hodolič, J. Fettich and K. Kairemo, Hypoxia PET Tracers in EBRT Dose Planning in Head and Neck Cancer, *Curr. Radiopharm.*, 2015, **8**(1), 32–37, DOI: **10.2174/1874471008666150316222400**.

11 J. A. Raleigh, A. J. Franko, C. J. Koch and J. L. Born, Binding of Misonidazole to Hypoxic Cells in Monolayer and Spheroid Culture: Evidence That a Side-Chain Label Is Bound as Efficiently as a Ring Label, *Br. J. Cancer*, 1985, **51**(2), 229–235, DOI: **10.1038/bjc.1985.33**.

12 E. Kjellsson Lindblom, A. Ureba, A. Dasu, P. Wersäll, A. J. G. Even, W. Elmpt, P. Lambin and I. Toma-Dasu, Impact of SBRT Fractionation in Hypoxia Dose Painting—Accounting for Heterogeneous and Dynamic Tumor Oxygenation, *Med. Phys.*, 2019, **46**(5), 2512–2521, DOI: **10.1002/mp.13514**.

13 V. Askoxylakis, J. Dinkel, M. Eichinger, B. Stieltjes, G. Sommer, L. G. Strauss, A. Dimitrakopoulou-Strauss, A. Kopp-Schneider, U. Haberkorn, P. E. Huber, M. Bischof, J. Debus and C. Thieke, Multimodal Hypoxia Imaging and Intensity Modulated Radiation Therapy for Unresectable Non-Small-Cell Lung Cancer: The HIL Trial, *Radiat. Oncol.*, 2012, **7**(1), 157, DOI: **10.1186/1748-717X-7-157**.

14 A. Salem, M.-C. Asselin, B. Reymen, A. Jackson, P. Lambin, C. M. L. West, J. P. B. O'Connor and C. Faivre-Finn, Targeting Hypoxia to Improve Non–Small Cell Lung Cancer Outcome, *JNCI, J. Natl. Cancer Inst.*, 2018, **110**(1), 14–30, DOI: **10.1093/jnci/djx160**.

15 J. G. Rajendran, K. R. G. Hendrickson, A. M. Spence, M. Muzi, K. A. Krohn and D. A. Mankoff, Hypoxia Imaging-Directed Radiation Treatment Planning, *Eur. J. Nucl. Med. Mol. Imaging*, 2006, **33**(S1), 44–53, DOI: **10.1007/s00259-006-0135-1**.

16 T. Liu, M. Karlsen, A. M. Karlberg and K. R. Redalen, Hypoxia Imaging and Theranostic Potential of [64Cu][Cu(ATSM)] and Ionic Cu(II) Salts: A Review of Current Evidence and Discussion of the Retention Mechanisms, *EJNMMI Res*, 2020, **10**(1), 33, DOI: **10.1186/s13550-020-00621-5**.

17 A. J. Weeks, R. L. Paul, P. K. Marsden, P. J. Blower and D. R. Lloyd, Radiobiological Effects of Hypoxia-Dependent Uptake of 64Cu-ATSM: Enhanced DNA Damage and Cytotoxicity in Hypoxic Cells, *Eur. J. Nucl. Med. Mol. Imaging*, 2010, **37**(2), 330–338, DOI: **10.1007/s00259-009-1305-8**.

18 H. Maeda, Tumor-Selective Delivery of Macromolecular Drugs via the EPR Effect: Background and Future Prospects, *Bioconjugate Chem.*, 2010, **21**(5), 797–802, DOI: **10.1021/bc100070g**.

19 W. Su, C. Chen, T. Wang, X. Li, Y. Liu, H. Wang, S. Zhao, C. Zuo, G. Sun and W. Bu, Radionuclide-Labeled Gold Nanoparticles for Nuclei-Targeting Internal Radio-Immunity Therapy, *Mater. Horiz.*, 2020, **7**(4), 1115–1125, DOI: **10.1039/C9MH01725A**.

20 L. Dziawer, P. Koźmiński, S. Męczyńska-Wielgosz, M. Pruszyński, M. Łyczko, B. Wąs, G. Celichowski, J. Grobelny, J. Jastrzębski and A. Bilewicz, Gold Nanoparticle Bioconjugates Labelled with 211At for Targeted Alpha Therapy, *RSC Adv.*, 2017, **7**(65), 41024–41032, DOI: **10.1039/C7RA06376H**.

21 Z. R. Goddard, M. J. Marín, D. A. Russell and M. Searcey, Active Targeting of Gold Nanoparticles as Cancer Therapeutics, *Chem. Soc. Rev.*, 2020, **49**(23), 8774–8789, DOI: **10.1039/D0CS01121E**.

22 M. Yafout, A. Ousaid, Y. Khayati and I. S. El Otmani, Gold Nanoparticles as a Drug Delivery System for Standard

Chemotherapeutics: A New Lead for Targeted Pharmacological Cancer Treatments, *Scientific African*, 2021, **11**, e00685, DOI: **10.1016/j.sciaf.2020.e00685**.

23 S. Mittal, R. Sharma, H. D. Sarma and M. B. Mallia, Hypoxia Targeting Lutetium-177-Labeled Nitroimidazole-Decorated Gold Particles as Cancer Theranostic Nanoplatforms, *Mater. Adv.*, 2022, **3**(4), 1993–1999, DOI: **10.1039/D1MA01123E**.

24 S. Banerjee, T. Das, S. Chakraborty and M. Venkatesh, Emergence and Present Status of Lu-177 in Targeted Radiotherapy: The Indian Scenario, *Radiochim. Acta*, 2012, **100**(2), 115–126, DOI: **10.1524/ract.2011.1843**.

25 J. S. Suk, Q. Xu, N. Kim, J. Hanes and L. M. Ensign, PEGylation as a Strategy for Improving Nanoparticle-Based Drug and Gene Delivery, *Adv. Drug Delivery Rev.*, 2016, **99**(Pt A), 28–51, DOI: **10.1016/j.addr.2015.09.012**.

26 R. Mundel, T. Thakur and M. Chatterjee, Emerging Uses of PLA-PEG Copolymer in Cancer Drug Delivery, *3 Biotech*, 2022, **12**(2), 41, DOI: **10.1007/s13205-021-03105-y**.

27 Y. Fu, Y. Ding, L. Zhang, Y. Zhang, J. Liu and P. Yu, Poly Ethylene Glycol (PEG)-Related Controllable and Sustainable Antidiabetic Drug Delivery Systems, *Eur. J. Med. Chem.*, 2021, **217**, 113372, DOI: **10.1016/j.ejmech.2021.113372**.

28 B. He, D. Yang, M. Qin, Y. Zhang, B. He, W. Dai, X. Wang, Q. Zhang, H. Zhang and C. Yin, Increased Cellular Uptake of Peptide-Modified PEGylated Gold Nanoparticles, *Biochem. Biophys. Res. Commun.*, 2017, **494**(1–2), 339–345, DOI: **10.1016/j.bbrc.2017.10.026**.

29 L. W. C. Ho, W.-Y. Yung, K. H. S. Sy, H. Y. Li, C. K. K. Choi, K. C.-F. Leung, T. W. Y. Lee and C. H. J. Choi, Effect of Alkylation on the Cellular Uptake of Polyethylene Glycol-Coated Gold Nanoparticles, *ACS Nano*, 2017, **11**(6), 6085–6101, DOI: **10.1021/acsnano.7b02044**.

30 S.-D. Li and L. Huang, Stealth Nanoparticles: High Density but Sheddable PEG Is a Key for Tumor Targeting, *J. Controlled Release*, 2010, **145**(3), 178–181, DOI: **10.1016/j.jconrel.2010.03.016**.

31 G. Zhang, Z. Yang, W. Lu, R. Zhang, Q. Huang, M. Tian, L. Li, D. Liang and C. Li, Influence of Anchoring Ligands and Particle Size on the Colloidal Stability and in Vivo Biodistribution of Polyethylene Glycol-Coated Gold Nanoparticles in Tumor-Xenografted Mice, *Biomaterials*, 2009, **30**(10), 1928–1936, DOI: **10.1016/j.biomaterials.2008.12.038**.

32 Y.-J. Gu, J. Cheng, C. W.-Y. Man, W.-T. Wong and S. H. Cheng, Gold-Doxorubicin Nanoconjugates for Overcoming Multidrug Resistance, *Nanomedicine*, 2012, **8**(2), 204–211, DOI: **10.1016/j.nano.2011.06.005**.

33 S. Mahalunkar, A. S. Yadav, M. Gorain, V. Pawar, R. Braathen, S. Weiss, B. Bogen, S. W. Gosavi and G. C. Kundu, Functional Design of pH-Responsive Folate-Targeted Polymer-Coated Gold Nanoparticles for Drug Delivery and in Vivo Therapy in Breast Cancer, *IJN*, 2019, **14**, 8285–8302, DOI: **10.2147/IJN.S215142**.

34 S. Mittal, R. Sharma, M. B. Mallia and H. D. Sarma, 68Ga-Labeled PET Tracers for Targeting Tumor Hypoxia: Role of Bifunctional Chelators on Pharmacokinetics, *Nucl. Med. Biol.*, 2021, **96–97**, 61–67, DOI: **10.1016/j.nucmedbio.2021.03.004**.

35 V. Torrisi, A. Graillot, L. Vitorazi, Q. Crouzet, G. Marletta, C. Loubat and J.-F. Berret, Preventing Corona Effects: Multiphosphonic Acid Poly(Ethylene Glycol) Copolymers for Stable Stealth Iron Oxide Nanoparticles, *Biomacromolecules*, 2014, **15**(8), 3171–3179, DOI: **10.1021/bm500832q**.

36 C. Brandenberger, C. Mühlfeld, Z. Ali, A.-G. Lenz, O. Schmid, W. J. Parak, P. Gehr and B. Rothen-Rutishauser, Quantitative Evaluation of Cellular Uptake and Trafficking of Plain and Polyethylene Glycol-Coated Gold Nanoparticles, *Small*, 2010, **6**(15), 1669–1678, DOI: **10.1002/smll.201000528**.

37 M. B. Mallia, S. Subramanian, A. Mathur, H. D. Sarma, M. Venkatesh and S. Banerjee, On the Isolation and Evaluation of a Novel Unsubstituted 5-Nitroimidazole Derivative as an Agent to Target Tumor Hypoxia, *Bioorg. Med. Chem. Lett.*, 2008, **18**(19), 5233–5237, DOI: **10.1016/j.bmcl.2008.08.069**.

38 M. B. Mallia, S. Subramanian, A. Mathur, H. D. Sarma and S. Banerjee, A Study on Nitroimidazole-99mTc(CO)3 Complexes as Hypoxia Marker: Some Observations towards Possible Improvement in in Vivo Efficacy, *Nucl. Med. Biol.*, 2014, **41**(7), 600–610, DOI: **10.1016/j.nucmedbio.2014.04.103**.

39 S. Barua and S. Mitragotri, Challenges Associated with Penetration of Nanoparticles across Cell and Tissue Barriers: A Review of Current Status and Future Prospects, *Nano Today*, 2014, **9**(2), 223–243, DOI: **10.1016/j.nantod.2014.04.008**.

40 X.-J. Dong, Z.-L. Zhang, L.-L. Wu, X.-Y. Ma, C.-M. Xu and D.-W. Pang, Coating Magnetic Nanospheres with PEG To Reduce Nonspecific Adsorption on Cells, *ACS Omega*, 2019, **4**(4), 7391–7399, DOI: **10.1021/acsomega.9b00245**.

41 L. Shi, J. Zhang, M. Zhao, S. Tang, X. Cheng, W. Zhang, W. Li, X. Liu, H. Peng and Q. Wang, Effects of Polyethylene Glycol on the Surface of Nanoparticles for Targeted Drug Delivery, *Nanoscale*, 2021, **13**(24), 10748–10764, DOI: **10.1039/D1NR02065J**.

42 H. S. Choi, B. I. Ipe, P. Misra, J. H. Lee, M. G. Bawendi and J. V. Frangioni, Tissue- and Organ-Selective Biodistribution of NIR Fluorescent Quantum Dots, *Nano Lett.*, 2009, **9**(6), 2354–2359, DOI: **10.1021/nl900872r**.

43 H. Soo Choi, W. Liu, P. Misra, E. Tanaka, J. P. Zimmer, B. Itty Ipe, M. G. Bawendi and J. V. Frangioni, Renal Clearance of Quantum Dots, *Nat. Biotechnol.*, 2007, **25**(10), 1165–1170, DOI: **10.1038/nbt1340**.

44 B. Du, X. Jiang, A. Das, Q. Zhou, M. Yu, R. Jin and J. Zheng, Glomerular Barrier Behaves as an Atomically Precise Bandpass Filter in a Sub-Nanometre Regime, *Nat. Nanotechnol.*, 2017, **12**(11), 1096–1102, DOI: **10.1038/nnano.2017.170**.

45 V. Naumenko, A. Nikitin, K. Kapitanova, P. Melnikov, S. Vodopyanov, A. Garanina, M. Valikhov, A. Ilyasov, D. Vishnevskiy, A. Markov, S. Golyshev, D. Zhukov, I. Alieva, M. Abakumov, V. Chekhonin and A. Majouga, Intravital Microscopy Reveals a Novel Mechanism of Nanoparticles Excretion in Kidney, *J. Controlled Release*, 2019, **307**, 368–378, DOI: **10.1016/j.jconrel.2019.06.026**.

46 X. Huang, L. Li, T. Liu, N. Hao, H. Liu, D. Chen and F. Tang, The Shape Effect of Mesoporous Silica Nanoparticles on Biodistribution, Clearance, and Biocompatibility *in Vivo*, *ACS Nano*, 2011, **5**(7), 5390–5399, DOI: **10.1021/nn200365a**.